Hindawi Publishing Corporation
Journal of Nanomaterials
Volume 2012, Article ID 958593, 6 pages
doi:10.1155/2012/958593

Research Article

Facile Hydrothermal Synthesis and Optical Properties of Monoclinic $CePO_4$ Nanowires with High Aspect Ratio

Nuengruethai Ekthammathat,[1] Titipun Thongtem,[1,2] Anukorn Phuruangrat,[3] and Somchai Thongtem[2,4]

[1] *Department of Chemistry, Faculty of Science, Chiang Mai University, Chiang Mai 50200, Thailand*
[2] *Materials Science Research Center, Faculty of Science, Chiang Mai University, Chiang Mai 50200, Thailand*
[3] *Department of Materials Science and Technology, Faculty of Science, Prince of Songkla University, Hat Yai, Songkhla 90112, Thailand*
[4] *Department of Physics and Materials Science, Faculty of Science, Chiang Mai University, Chiang Mai 50200, Thailand*

Correspondence should be addressed to Titipun Thongtem, ttpthongtem@yahoo.com
and Anukorn Phuruangrat, phuruangrat@hotmail.com

Received 14 April 2012; Accepted 10 July 2012

Academic Editor: Yanqiu Zhu

One-dimensional cerium phosphate ($CePO_4$) nanowires (NWs) were successfully synthesized by a facile and simple hydrothermal method at 200°C for 12 h, using $Ce(NO_3)_3 \cdot 6H_2O$ and $Na_3PO_4 \cdot 12H_2O$ as starting materials, and followed by pH adjusting to be 1–3 using HNO_3 (conc.). Phase, morphologies, and vibration modes of the as-synthesized $CePO_4$ products, characterized by XRD, SEM, TEM, and FTIR, were proved to be perfect and uniform monoclinic $CePO_4$ nanowires with aspect ratio of more than 250 for the product synthesized in the solution with the pH of 1. The UV-visible and photoluminescence (PL) spectrometers were used to investigate optical properties of the as-synthesized monoclinic $CePO_4$ nanowires.

1. Introduction

Since the discovery of carbon nanotubes by Iijima in 1990, a number of one-dimensional (1D) nanotubes, nanorods, and nanowires, have widely attracted interest for worldwide scientists, due to their novel physical and chemical properties caused by their low-dimensional and quantum-sized effects for different applications. In addition, these 1D nanomaterials can play an important role in functional nanodevices for light emitting diodes (LEDs), solar cells, single-electron transistors, lasers, and fluorescence for biological labels. Controling the synthesis of anisotropic nanostructured materials may therefore bring towards some unique properties and further enhance performances for a variety of applications [1–3].

Rare earth phosphate materials with unique 4f-5d and 4f-4f electronic transition have been widely used as high-performance luminescent devices, magnetic materials, catalysts, time-resolved fluorescence labels, and other functional materials. They are well known for the production of phosphor, sensor, and heat-resistant materials. Among them, $CePO_4$ as well as its solid solutions is able to be used as highly efficient emitters for green light of luminescent devices. The monoclinic $CePO_4$ monazite, one of the most stable materials although at a temperature as high as 1200 K, is appropriate for heat-resistant ceramic applications. It exists for billions of years by forming solid solutions with tetravalent actinide ions, such as U^{4+} and Th^{4+}. Thus it is a promising material for nuclear waste storage. But for hexagonal $CePO_4$, it is able to apply for tribological applications due to its natural layered structure [2–6].

In this paper, synthesis and formation mechanism of monoclinic $CePO_4$ nanowires (NWs) with high aspect ratio by a hydrothermal method without the use of surfactant and template as morphological controlling agents were reported. This method is simple, inexpensive, highly effective, and appropriate for synthesizing of other 1D nanomaterials.

2. Experiment

All reagents, $Ce(NO_3)_3 \cdot 6H_2O$, $Na_3PO_4 \cdot 12H_2O$, and HNO_3, bought from Sigma-Aldrich Co. LLC., were analytical grade

and used without further purification. For a typical synthesis of monoclinic $CePO_4$ NWs, 0.003 mol $Ce(NO_3)_3 \cdot 6H_2O$ was dissolved in 10 mL distilled water with the subsequent adding of 10 mL 0.003 M $Na_3PO_4 \cdot 12H_2O$ solution. The solution pH was adjusted to 1, 1.5, 2, and 3 using HNO_3 (conc.). Then, each of these solutions was transferred into Teflon containers, which were put in home-made stainless steel autoclaves. The autoclaves were tightly closed, heated at 200°C for 12 h in an electric oven, and left naturally cool down to room temperature. Then the as-synthesized precipitates were separated by filtration, washed with deionized water several times and ethanol, and dried at 70°C for 12 h. The final products appeared as light green solid powder.

The crystalline phases and crystalline degree of the as-synthesized nanostructured products were analyzed by X-ray diffractometer (XRD, Philips X'Pert MPD) operating at 45 kV 35 mA and using Cu K_α line in $2\theta = 10^\circ - -60^\circ$. The morphology investigation was carried out by field emission scanning electron microscope (FE-SEM, JEOL JSM-6335F) operating at 15 kV, transmission electron microscope (TEM, JEOL JEM-2010), and high resolution transmission electron microscope (HRTEM) using LaB_6 electron gun operated at 200 kV. The samples for EM analysis were prepared by sonicating of dry products in absolute ethanol for 15 min. For SEM analysis, the solutions were dropped on aluminum stubs, dried in ambient atmosphere, and coated by Au sputtering to increase electrical conductivity. But for TEM analysis, 3–5 drops of the suspensions were put on carbon-coated copper grids which were dried in ambient atmosphere. Fourier transform infrared (FTIR, *PerkinElmer* RX 1) spectrophotometer was carried out in the range of 4000 to 400 cm^{-1} with 4 cm^{-1} resolution. Their optical properties were studied by a UV-visible (UV-vis) spectrometer (Lambda 25 PerkinElmer) using a UV lamp with the resolution of 1 nm and a fluorescence spectrophotometer (LS50BPerkinElmer) using 450 W Xe lamp with 0.2 nm resolution.

3. Results and Discussion

Phase of the product was characterized by X-ray powder diffraction (XRD) as shown in Figure 1. The XRD pattern was readily specified as monoclinic $CePO_4$ structure of the JCPDS database number 32-0199 [7]. There were no detection of any peaks of impurities of CeO_2 and hexagonal $CePO_4$ in this paper. Its lattice parameters (a, b, and c) and volume (V) of unit cell were calculated from the equations for monoclinic structure below

$$\frac{1}{d^2} = \frac{1}{\sin^2\beta}\left[\frac{h^2}{a^2} + \frac{k^2\sin^2\beta}{b^2} + \frac{l^2}{c^2} - \frac{2hl\cos\beta}{ac}\right], \quad (1)$$

$$V = abc\sin\beta,$$

where h, k, and l are the Miller indices, d is the plane spacing, and β is the angle between the a and c axes (103.46°) [8]. The calculated lattice parameters of monoclinic $CePO_4$ structure were $a = 6.7852$ Å, $b = 7.0802$ Å, and $c = 6.4523$ Å—in good accordance with those of the JCPDS database ($a = 6.8004$ Å, $b = 7.0231$ Å, and $c = 6.4717$ Å). The calculated cell volume of the as-synthesized $CePO_4$ NWs was 301.45 $Å^3$, higher than that of its bulk of 300.60 $Å^3$. The increase in the cell volume indicated that lattice of the NWs was more distorted than that of their bulk [9, 10].

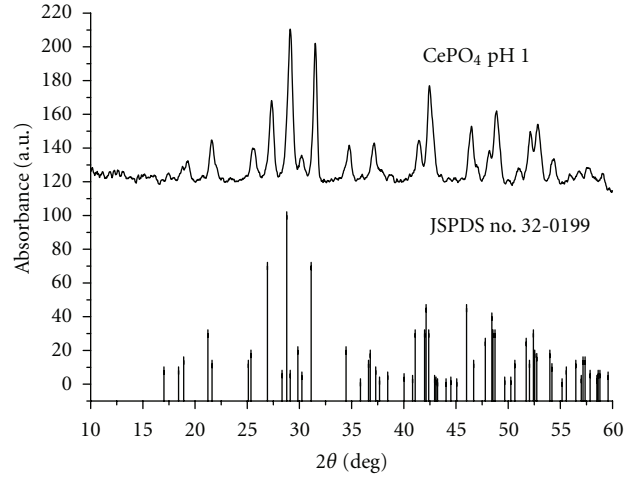

Figure 1: XRD pattern of $CePO_4$ NWs synthesized by the 200°C and 12 h hydrothermal reaction of the solution with the pH of 1, compared with the JCPDS database.

Table 1: The 1D $CePO_4$ products synthesized by the 200°C and 12 h hydrothermal reaction of the solutions with different pH values.

Solution pH	Length (μm)	Diameter (nm)	Aspect ratio
1	5.00–7.00	20	250–350
1.5	2.00–5.00	20	100–250
2	1.00–1.50	15	67–100
3	0.20–0.30	10	20–30

Figure 2 shows FTIR spectra of $CePO_4$ NWs synthesized by the hydrothermal reaction at the pH of 1 adjusted by HNO_3 solution. The vibrations of $CePO_4$ NWs were due to the PO_4^{3-} tetrahedrons, belonging to the $A_1(R) + E(R) + 2F_2(IR + R)$. The $\nu_1(A_1)$ (symmetric stretching mode) and $\nu_2(E)$ (symmetric bending mode) are Raman (R) active, and the $\nu_3(F_2)$ (asymmetric stretching mode) and $\nu_4(F_2)$ (asymmetric bending mode) are R and IR doubly active modes. The symmetry of PO_4^{3-} ions in the $CePO_4$ crystals decreases from T_d to C_1, and thus the non-IR modes become IR active [10]. The broad band at 3460 cm^{-1} was assigned as the O–H stretching vibration of water molecules, adsorbed on surface of the product. The bands at 1200–400 cm^{-1} wavenumbers were assigned as the vibrations of PO_4^{3-} groups. Those centered at 1052 cm^{-1} were specified as the asymmetric stretching vibrations of the PO_4^{3-} groups and those at 609 cm^{-1} and 536 cm^{-1} were as the O–P–O bending vibrations. Four medium-intensity peaks between 700 and 400 cm^{-1} were caused by bending of P–O links in PO_4^{3-} distorted tetrahedrons. The P–O stretching peak was split bands due to the removal of degeneracy of tetrahedral vibrations, corresponding to the characteristic peaks of phosphate groups of monoclinic cerium phosphate. In the monazite monoclinic phase, the tetrahedral phosphate groups are distorted in the nine fold coordination of lanthanide atoms

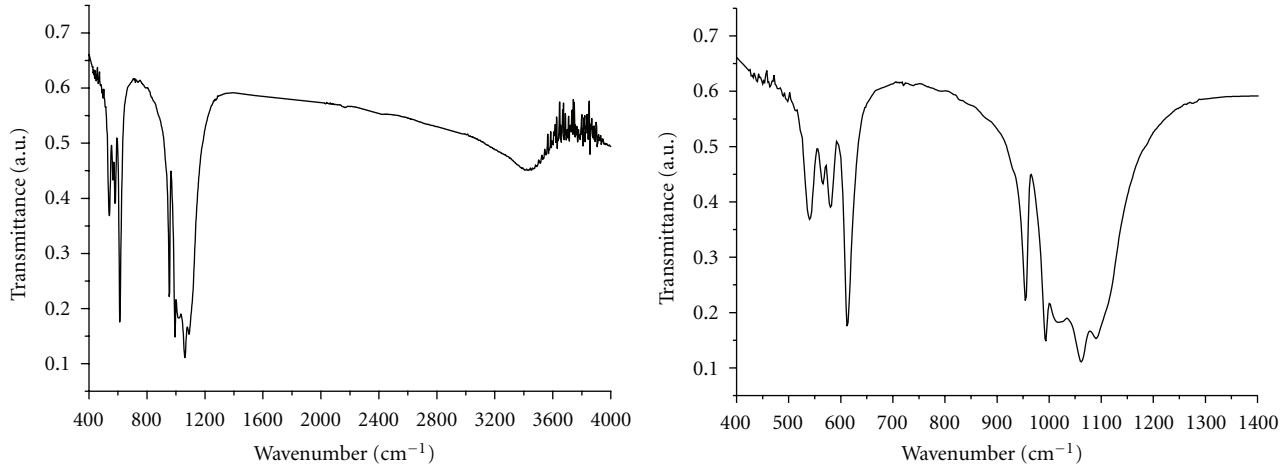

Figure 2: FTIR spectra of $CePO_4$ NWs synthesized by the 200°C and 12 h hydrothermal reaction of the solution with the pH of 1. (a) 4000–400 cm^{-1} and (b) 1400–400 cm^{-1}.

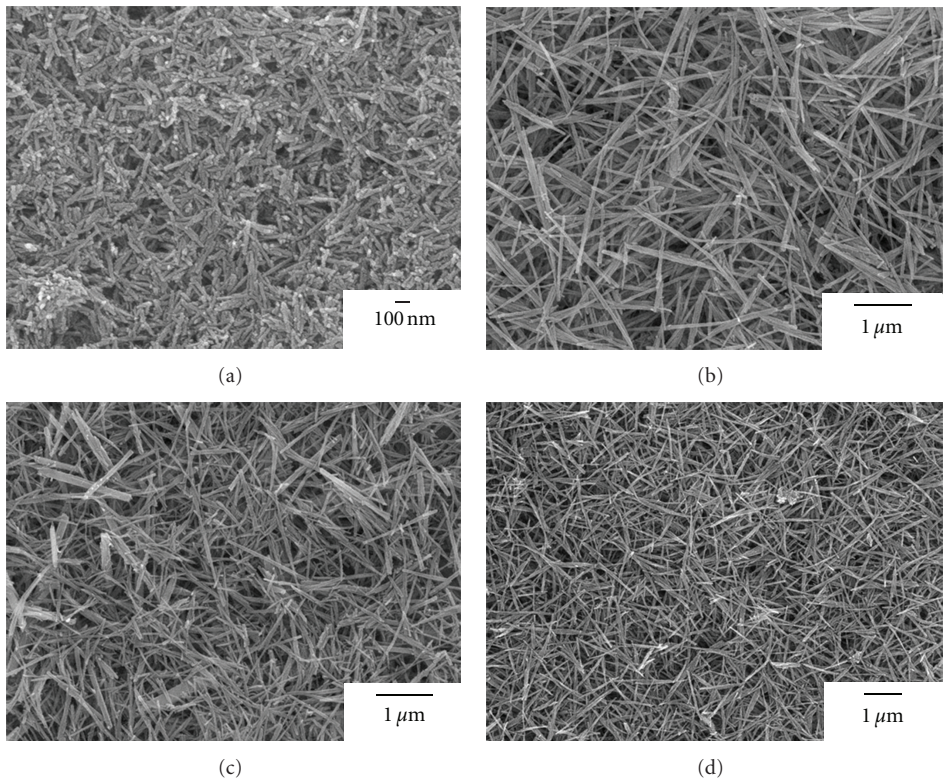

Figure 3: SEM images of $CePO_4$ synthesized by the 200°C and 12 h hydrothermal reaction of the solution with the pH of (a–d) 3, 2, 1.5, and 1, respectively.

Table 2: Individual component of PL spectrum of $CePO_4$ NWs. Emission intensities were calculated from areas under the corresponding curves.

Individual component	Emission wavelength (nm)	Area under curve	Intensity (%)
P1	361.36 (ultraviolet)	381.56	6.00
P2	388.24 (ultraviolet)	1505.29	23.65
P3	438.46 (violet)	2449.46	38.49
P4	482.52 (blue)	160.49	2.52
P5	505.94 (green)	1867.22	29.34

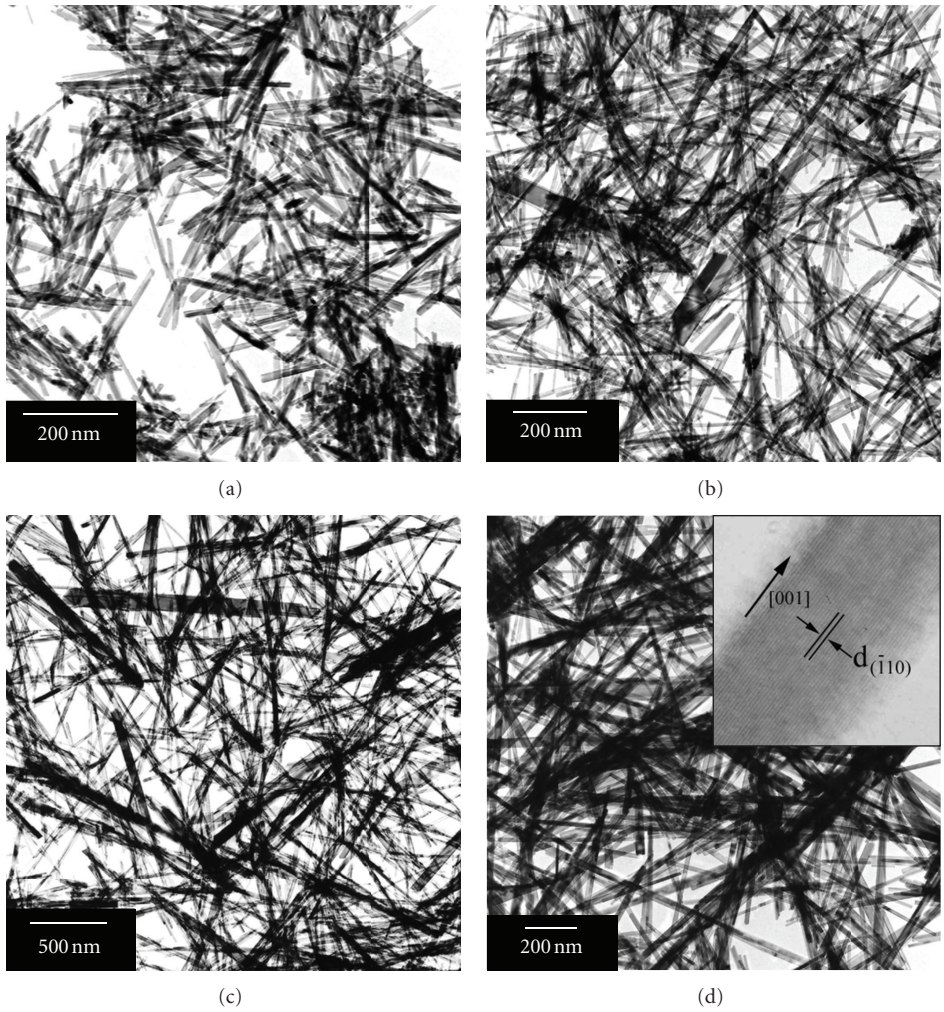

Figure 4: TEM images of $CePO_4$ synthesized by the 200°C and 12 h hydrothermal reaction of the solution with the pH of (a–d) 3, 2, 1.5, and 1, respectively. Inserted HRTEM image of (d) shows the growth direction and crystallographic plane of the NW.

and the phosphate absorptions are split accordingly. The stretching modes appeared as a cluster of very strong peaks at 954, 993, 1052, and 1092 cm^{-1}. The adsorption of NO_3^- anions (1380 and 878 cm^{-1}) from the precursor was not detected, indicating that the product was very pure phase [10–13].

The product morphology (Figure 3) was characterized by a scanning electron microscope (SEM), and was able to specify the evolution in the length of one-dimensional $CePO_4$ product-influenced by pH of the solutions. Only the monoclinic $CePO_4$ nanorods with 200 to 300 nm long and 10 nm in diameter were synthesized by the 200°C and 12 h hydrothermal reaction of the precursor solution with the pH of 3. Upon adjusting the pH values to 2 and 1.5, some $CePO_4$ nanorods were transformed into $CePO_4$ nanowires (NWs) with 1 to 5 μm in length and 15 to 20 nm in diameter. At the precursor solution pH of 1, the whole $CePO_4$ NWs with aspect ratio > 250 were synthesized. The aspect ratios for different solution pH were summarized in Table 1, which showed the influence of pH values on the lengths and diameters of 1D $CePO_4$. In this paper, uniform $CePO_4$ NWs with high aspect ratio were successfully synthesized by the 200°C and 12 h hydrothermal reaction of the solution with the pH of 1.

To further show the real morphologies of the as-synthesized monoclinic $CePO_4$ at the pH of 1–3, the products were characterized by a transmission electron microscope (TEM) (Figure 4). At the pH of 3, the product was structurally uniform nanorods. Their average diameter was 10 nm and length was up to 300 nm. Mixed nanowires and nanorods were detected at the pH of 2 and 1.5. The whole $CePO_4$ NWs with longer than 5 μm and diameter of 20 nm were synthesized at the pH of 1. The growth direction of monoclinic $CePO_4$ NWs was investigated by high resolution transmission electron microscope (HRTEM) as shown in the inset of Figure 4(d). It shows that the lattice spacing was about 4.81 Å, corresponding to the (−110) plane, with the growth direction of single monoclinic $CePO_4$ crystal along the [001] direction-parallel to the (−110) plane.

In general, the anisotropic growth of one-dimensional materials was driven by several factors such as surface energy, structure, electrostatic force, and surfactant. In this paper,

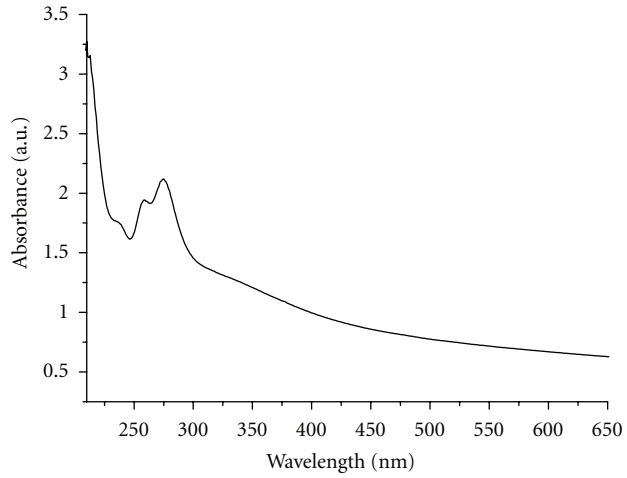

FIGURE 5: UV-visible spectrum of $CePO_4$ NWs synthesized by the 200°C and 12 h hydrothermal reaction of the solution with the pH of 1.

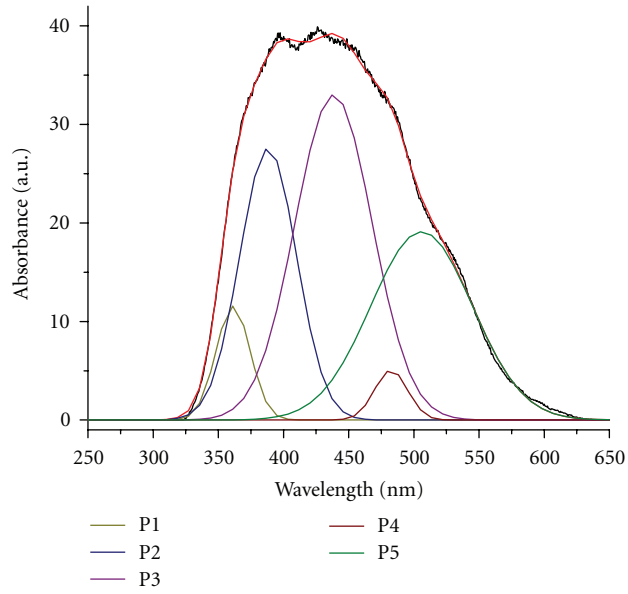

FIGURE 6: PL spectrum of $CePO_4$ NWs synthesized by the 200°C and 12 h hydrothermal reaction of the solution with the pH of 1. Centers of the five deconvoluted peaks from left to right are in sequence as P1, P2, P3, P4, and P5.

the anisotropic $CePO_4$ NWs was controlled by the chemical potential. The faster ionic migration usually promoted the reversible pathway between fluid and solid phases, leaving ions to reside in the right positions of crystal lattice [14]. The formation mechanism of $CePO_4$ NWs is able to explain as follows:

$$PO_4^{3-} + nH^+ \longrightarrow H_nPO_4^{(3-n)-}$$

$$Ce^{3+} + H_nPO_4^{(3-n)-} \longrightarrow CePO_4 \text{ (light green precipitates)} + nH^+ \quad (2)$$

$Ce(NO_3)_3 \cdot 6H_2O$ and $Na_3PO_4 \cdot 12H_2O$ were mixed in distilled water, with the following of pH adjusting using HNO_3 (conc.). During the hydrothermal treatment of the solution with the pH of 1, the clear colorless solution was heated up under high pressure. Concurrently, the Ce^{3+} and $H_nPO_4^{(3-n)-}$ chemical potentials were raised up, including the faster ionic migration in the solution. During cooling, these ions combined to form light green precipitates of monoclinic $CePO_4$ NWs—in accordance with the reports of Zhang and Guan [3].

The optical properties of $CePO_4$ NWs hydrothermally synthesized in the solution with the pH of 1 were investigated by UV-visible and photoluminescence (PL) spectroscopy. The $CePO_4$ NWs for the analyses were ultrasonically dispersed in absolute ethanol for 10 min. Their UV-visible absorption spectrum (Figure 5) is in the range of 220 to 650 nm. The absorption was detected as a strong band in the ultraviolet range, caused by the f–d electron transition of Ce^{3+} atoms in the lattice. It shows the major absorption peak at 274 nm coupled with a small shoulder at 257 nm. These bands were overlapping as the excited states were strongly split by the crystal field. Moreover, these results are in consistent with the data for transition from the Ce^{3+} $^2F_{5/2}(4f^1)$ ground state to the five crystal field split levels of the Ce^{3+} ^2D $(5d^1)$ excited states, namely, the $^2D_{5/2}$ and $^2D_{3/2}$ [9, 15].

Figure 6 shows the PL spectrum at room temperature of $CePO_4$ NWs using the excitation wavelength of 325 nm. It displays a broad emission peak of the $CePO_4$ NWs over the 325 to 625 nm range. To estimate the contribution of each, it was necessary to deconvolute the PL spectrum. By using the Gaussian analysis, the deconvoluted results shows that the PL profile was at the best for five deconvoluted peaks. The first, second, and third were in the ultraviolet spectrum, the fourth in the blue range, and the fifth in the green wavelength. Each component represents different types of electronic transition, linked with the atomic arrangement and surface defects. The PL spectrum exhibits strong emission peaks centered at 388.24 nm (ultraviolet) and 438.46 nm (violet) [13, 16, 17]. Emission wavelength, color, and intensity of each component of $CePO_4$ NWs are shown in Table 2. The strongest intensity of the PL spectrum for $CePO_4$ NWs corresponded to the 438.46 nm violet wavelength with 38.49% of the whole emission.

4. Conclusions

In summary, uniform $CePO_4$ NWs with aspect ratio of more than 250 were synthesized by the facile hydrothermal method. Their formation mechanism was also discussed in this paper. Different lengths and sizes of $CePO_4$ products were influenced by the pH values. The uniform monoclinic $CePO_4$ NWs were synthesized in the solution with the pH of 1. These NWs show the strong absorption in the ultraviolet range due to the f–d electron transition of Ce^{3+} atoms in crystal lattice. Their PL emission shows a broad band of 325 to 625 nm range with the strongest emission at 438.46 nm in the violet region.

Acknowledgments

The authors wish to thank the Thailand's Office of the Higher Education Commission for providing financial support through the National Research University Project for Chiang Mai University (CMU) and the Human Resource Development Project in Science Achievement Scholarship of Thailand (SAST), and the Faculty of Science Research Fund, Prince of Songkla University (PSU), including the Graduate School of CMU through the general support.

References

[1] L. Qian, W. Du, Q. Gong, and X. Qian, "Controlled synthesis of light rare earth phosphate nanowires via a simple solution route," *Materials Chemistry and Physics*, vol. 114, no. 1, pp. 479–484, 2009.

[2] W. Fan, W. Zhao, L. You et al., "A simple method to synthesize single-crystalline lanthanide orthovanadate nanorods," *Journal of Solid State Chemistry*, vol. 177, no. 12, pp. 4399–4403, 2004.

[3] Y. Zhang and H. Guan, "Hydrothermal synthesis and characterization of hexagonal and monoclinic $CePO_4$ single-crystal nanowires," *Journal of Crystal Growth*, vol. 256, no. 1-2, pp. 156–161, 2003.

[4] J. Bao, R. Yu, J. Zhang et al., "Low-temperature hydrothermal synthesis and structure control of nano-sized $CePO_4$," *CrystEngComm*, vol. 11, no. 8, pp. 1630–1634, 2009.

[5] Y. B. Yin, X. Shao, L. M. Zhao, and W. Z. Li, "Synthesis and characterization of $CePO_4$ nanowires *via* microemulsion method at room temperature," *Chinese Chemical Letters*, vol. 20, no. 7, pp. 857–860, 2009.

[6] M. Cao, C. Hu, Q. Wu, C. Guo, Y. Qi, and E. Wang, "Controlled synthesis of $LaPO_4$ and $CePO_4$ nanorods/nanowires," *Nanotechnology*, vol. 16, no. 2, pp. 282–286, 2005.

[7] "Powder Diffract. File," JCPDS-ICDD, 12 Campus Boulevard, Newtown Square, PA 19073-3273, U.S.A., 2001.

[8] C. Suryanarayana and M. G. Norton, *X-Ray Diffraction: A Practical Approach*, Plenum Press, New York, NY, USA, 1998.

[9] Y. P. Fang, A. W. Xu, R. Q. Song et al., "Systematic synthesis and characterization of single-crystal lanthanide orthophosphate nanowires," *Journal of the American Chemical Society*, vol. 125, no. 51, pp. 16025–16034, 2003.

[10] K. Wang, J. Zhang, J. Wang et al., "Growth defects and infrared spectra analysis of $CePO_4$ single crystals," *Journal of Applied Crystallography*, vol. 38, no. 4, pp. 675–677, 2005.

[11] N. Sumaletha, K. Rajesh, P. Mukundan, and K. G. K. Warrier, "Environmentally benign sol-gel derived nanocrystalline rod shaped calcium doped cerium phosphate yellow-green pigment," *Journal of Sol-Gel Science and Technology*, vol. 52, no. 2, pp. 242–250, 2009.

[12] L. Ma, W. X. Chen, Y. F. Zheng, and Z. D. Xu, "Hydrothermal growth and morphology evolution of $CePO_4$ aggregates by a complexing method," *Materials Research Bulletin*, vol. 43, no. 11, pp. 2840–2849, 2008.

[13] M. Yang, H. You, Y. Zheng et al., "Hydrothermal synthesis and luminescent properties of novel ordered sphere $CePO_4$ hierarchical architectures," *Inorganic Chemistry*, vol. 48, no. 24, pp. 11559–11565, 2009.

[14] G. Fasol, "Nanowires: small is beautiful," *Science*, vol. 280, no. 5363, pp. 545–546, 1998.

[15] F. Zhang and S. S. Wong, "Ambient large-scale template-mediated synthesis of high-aspect ratio single-crystalline, chemically doped rare-earth phosphate nanowires for bioimaging," *ACS Nano*, vol. 4, no. 1, pp. 99–112, 2010.

[16] M. Guan, J. Sun, T. Shang, Q. Zhou, J. Han, and A. Ji, "A facile synthesis of cerium phosphate nanofiber by solution-solid method," *Journal of Materials Science & Technology*, vol. 26, no. 1, pp. 45–48, 2010.

[17] G. Li, K. Chao, H. Peng, K. Chen, and Z. Zhang, "Facile synthesis of $CePO_4$ nanowires attached to CeO_2 octahedral micrometer crystals and their enhanced photoluminescence properties," *The Journal of Physical Chemistry C*, vol. 112, no. 42, pp. 16452–16456, 2008.